

# Unveiling Smart Water Treatment Technology by Heterocyclic Nitrogen-based B<sub>7</sub>N<sub>6</sub> Nanostructure through Computer-aided Material Modelling

Fateme Mollaamin<sup>1,\*</sup> 

<sup>1</sup> Department of Biomedical Engineering, Faculty of Engineering and Architecture, Kastamonu University, Kastamonu, Turkey

\* Correspondence: [fmollaamin@kastamonu.edu.tr](mailto:fmollaamin@kastamonu.edu.tr);

Received: 11.10.2024; Accepted: 27.07.2025; Published: 30.09.2025

**Abstract:** This article aims to assess a graphitic-like monolayer boron nitride (B<sub>7</sub>N<sub>6</sub>) nanosheet as an effective adsorbent for pollutants in water, including organic molecules of CH<sub>3</sub>OH, CHBr<sub>2</sub>, NaOH, and NH<sub>3</sub>. The changes of charge density (Q) have shown a more important charge transfer toward B<sub>7</sub>N<sub>6</sub> nanosheet, which acts as the electron acceptor, while CH<sub>3</sub>OH, CHBr<sub>2</sub>, NaOH, and NH<sub>3</sub> molecules act as the electron donors. Based on Nuclear quadrupole resonance (NQR) analysis, B<sub>7</sub>N<sub>6</sub> nanosheet represents enough capability for adsorbing CH<sub>3</sub>OH, CHBr<sub>2</sub>, NaOH, and NH<sub>3</sub> through electric potential values of hydrogen, carbon, nitrogen, oxygen, bromine, and boron atoms during adsorption of organic molecules (adsorbates) on B<sub>7</sub>N<sub>6</sub> nanosheet (adsorbent). NMR spectroscopy exhibited the remarkable peaks around carbon, nitrogen, oxygen, and bromine atoms through the adsorption procedure of CH<sub>3</sub>OH, CHBr<sub>2</sub>, NaOH, and NH<sub>3</sub> on the B<sub>7</sub>N<sub>6</sub> nanosheet, with the fluctuations in the chemical shielding behaviors of isotropic and anisotropic attributes. All the measured thermodynamic parameters extracted from IR spectra have exhibited the most stable energy for CHBr<sub>2</sub> and CBr<sub>2</sub>– B<sub>7</sub>N<sub>6</sub>. This work can evaluate the adsorption of different organic contaminants of CH<sub>3</sub>OH, CHBr<sub>2</sub>, NaOH, and NH<sub>3</sub> on the B<sub>7</sub>N<sub>6</sub>-based nanosheet and, correspondingly, can introduce helpful information for using this nanomaterial in water treatment. This approach can support the safe and sustainable evolution of smart water instruments.

**Keywords:** Clean water; B<sub>7</sub>N<sub>6</sub> nanosheet; adsorption; DFT.

© 2025 by the authors. This article is an open-access article distributed under the terms and conditions of the Creative Commons Attribution (CC BY) license (<https://creativecommons.org/licenses/by/4.0/>), which permits unrestricted use, distribution, and reproduction in any medium, provided the original work is properly cited. The authors retain copyright of their work, and no permission is required from the authors or the publisher to reuse or distribute this article, as long as proper attribution is given to the original source.

## 1. Introduction

Semiconductor materials are mainly prepared from the elements in groups II to VI of the periodic table [1]. In the compound in the group III–V, each atom of group III is bonded to four atoms of group V for attaining an octet in the valence band, when the valence charge from an atom of group V transfers toward an atom of group III and cultivates partial ionic bonding to the crystal surface [2].

A variety of organic and inorganic pollutants containing pharmaceuticals, endocrine-disrupting compounds, dye chemicals, which are usually separated into organic-inorganic and synthetic-natural groups, and heavy metals such as Cu, Cr, Zn, Ni, Pb, Hg, Cd, As, and Ag have often been discovered in many drinking water sources and wastewaters worldwide [3-6].

Various methods have been applied to remove different inorganic and organic pollutants in water, such as chemical precipitation, photocatalytic oxidation, membrane filtration, coagulation, ion exchange, and adsorption [7-9].

Adsorption is one of the most generally employed removal methods due to its special traits like selectivity, simplicity, and cost-efficiency [10,11].

Recently, 2D or 3D nanomaterials with unique specifications have been investigated as engaged adsorbents for the impressive removal of different environmental chemicals such as carbon nanotubes, graphene surfaces, MOFs, and boron nitrides with thin shapes, principal specific surface area, and powerful functional situations [12-16].

Boron nitride nanomaterials have been used owing to their unique characteristics, such as eco-friendly attributes for pollutant adsorption, large surface area, high chemical and mechanical strength, and semiconducting property [17-21].

Boron nitride nanomaterials usually exhibit semi-leading behavior, which is considered a proper alternative to carbon nanotubes. The properties of boron and nitrogen atoms, which are the first neighbors of carbon in the periodic table, make boron nitride an interesting subject of numerous studies [22-28].

In recent years, different research on the adsorption of chemical contaminants and applying various boron nitride nanomaterials as adsorbents for water purification has been studied [29-44].

Various physical shapes of boron nitride ( $B_7N_6$ )-based nano adsorbents such as nanoparticles, fullerenes, nanotubes, nanofibers, nanoribbons, nanosheets, nanomeshes, nanoflowers, and hollow spheres have been broadly considered possible adsorbents owing to their exceptional characteristics such as large surface area, structural variability, great chemical/mechanical strength, abundant structural defects, high reactive sites, and functional groups [45-48].

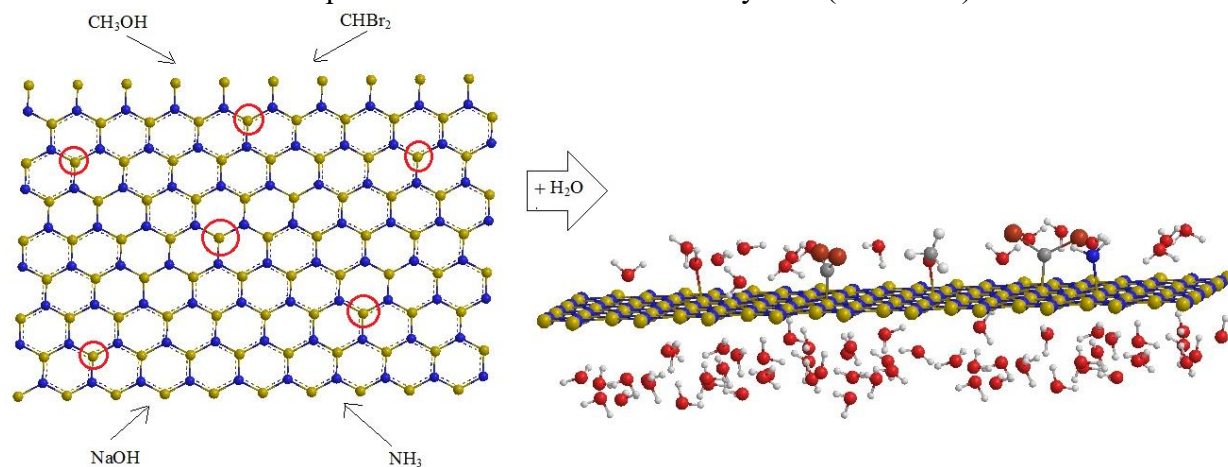
Particularly, this research work aims to assess the influences of adsorbent properties of boron nitride ( $B_7N_6$ ) nanosheet (charge transfer, electromagnetic, thermodynamic, surface area, and functional group) on contaminant removal, and examine the removal of selected contaminants of  $CH_3OH$ ,  $CHBr_2$ ,  $NaOH$ , and  $NH_3$  during the adsorption process.

## 2. Compounds and Computational Approach

In this research article, the simulated calculations have been performed in GaussView 6.06.16 [49] and calculated by Gaussian 16, Revision C.01 [50] using the DFT method. Recently, usage of computed density functional theory Kohn–Sham (DFT-KS) orbitals and eigenvalues has achieved augmented popularity owing to their capability to depict and foretell physico-chemical attributes of large systems. Our fondness in this issue has been to engage the exchange-correlation hybrid functional B3LYP (Becke, [51] 3-parameter [52], Lee–Yang–Parr [53]) to assess the geometry of large donor–acceptor assemblies pursued by comparison of the computed KS orbital energies with measured thermochemical and spectral specifications.

The [Perdew–Burke–Ernzerhof] "PBE" functional with high-precision generalized gradient approximation "GGA" has been employed to achieve more authentic results [54]. The functionals are related to PBE exchange and correlation. While the uncalibrated GGA-based functionals usually put out extremely poor thermochemical information, calibration authorizes an extensive reform, with only a small decline of reaction barriers. Therefore, an optimized B3LYP-based local-hybrid functional has been found that is a substantial improvement over the underlying global hybrids.

Every simulated group contains a graphite-like sheet of length 25 Å with a bond length of 1.95 Å for the B<sub>7</sub>N<sub>6</sub> nanosheet with a single CH<sub>3</sub>OH, CHBr<sub>2</sub>, NaOH, or NH<sub>3</sub> molecule adsorbed onto it (Scheme 1). In addition, the multiplicity of 1 and global charges of 0 have been considered as the input condition for the simulated system (Scheme 1).



**Scheme 1.** "Langmuir" adsorption of CH<sub>3</sub>OH, CHBr<sub>2</sub>, NaOH, and NH<sub>3</sub> on the B<sub>7</sub>N<sub>6</sub> nanosheet.

The charge transfer between adsorbates of CH<sub>3</sub>OH, CHBr<sub>2</sub>, NaOH, and NH<sub>3</sub> and the adsorbent of the B<sub>7</sub>N<sub>6</sub> nanosheet is calculated due to the Bader charge analysis [55]. This method can measure charge accumulation from the charge of each atom in the complex model. Finally, the total adsorption charge transfer can be obtained as a formula:

$$\Delta Q_t = Q_2 - Q_1 \quad (1)$$

Where Q<sub>1</sub> and Q<sub>2</sub> remark the charge distribution of CH<sub>3</sub>OH, CHBr<sub>2</sub>, NaOH, and NH<sub>3</sub> on the B<sub>7</sub>N<sub>6</sub> surface before and after adoption, respectively, as a matter of fact, positive ΔQ<sub>t</sub> indicates that electrons are transferred from CH<sub>3</sub>OH, CHBr<sub>2</sub>, NaOH, and NH<sub>3</sub> to the surface of the B<sub>7</sub>N<sub>6</sub> nanosheet, and the adsorbent acts as an electron acceptor [56,57].

The adsorption of CH<sub>3</sub>OH, CHBr<sub>2</sub>, NaOH, and NH<sub>3</sub> molecules on the surface of B<sub>7</sub>N<sub>6</sub> nanosheet was defined by the theory "Langmuir" isotherm (Scheme 1) [58-68].

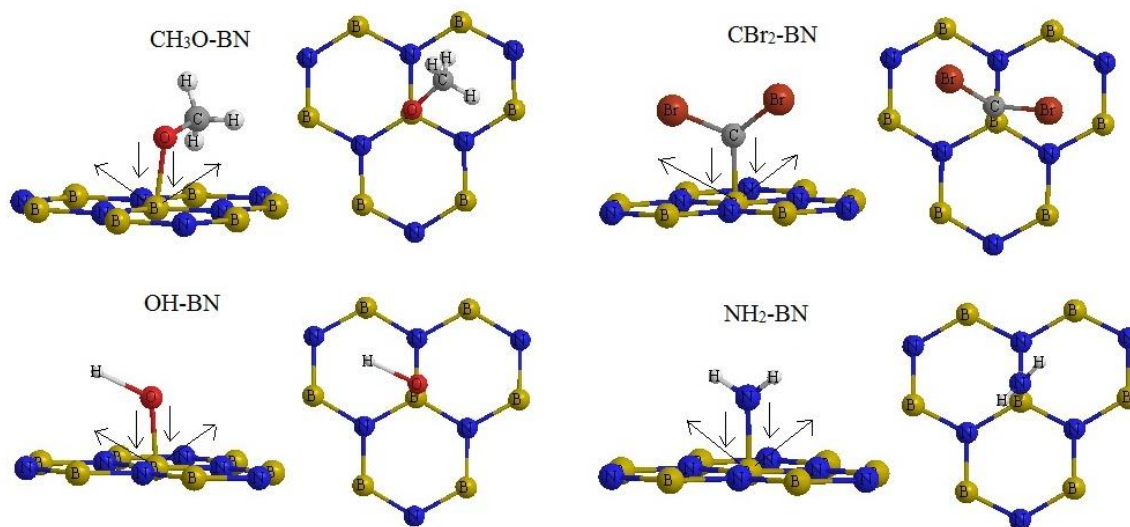
The changes in charge density analysis in the adsorption process have illustrated that B<sub>7</sub>N<sub>6</sub> nanosheet shows the Bader charge of -0.325e before adsorption of CH<sub>3</sub>OH, CHBr<sub>2</sub>, NaOH, NH<sub>3</sub>, and -0.292e, -0.325e, -0.298e, -0.396e after adsorption of CH<sub>3</sub>OH, CHBr<sub>2</sub>, NaOH, NH<sub>3</sub>, respectively. Therefore, the changes of charge density for "Langmuir" adsorption of CH<sub>3</sub>OH, CHBr<sub>2</sub>, NaOH, NH<sub>3</sub> on B<sub>7</sub>N<sub>6</sub> surface alternatively are ΔQ<sub>CH<sub>3</sub>OH@ B<sub>7</sub>N<sub>6</sub></sub> = +0.033 > ΔQ<sub>NaOH@ B<sub>7</sub>N<sub>6</sub></sub> = +0.027 > ΔQ<sub>CHBr<sub>2</sub>@ B<sub>7</sub>N<sub>6</sub></sub> = 0 > ΔQ<sub>NH<sub>3</sub>@ B<sub>7</sub>N<sub>6</sub></sub> = -0.071.

The values of changes of charge density have shown a more important charge transfer for B<sub>7</sub>N<sub>6</sub> nanosheet (adsorbent), which acts as the electron acceptor, while CH<sub>3</sub>OH, CHBr<sub>2</sub>, NaOH, and NH<sub>3</sub> molecules (adsorbates) act as the stronger electron donors through adsorption on the graphitic-like B<sub>7</sub>N<sub>6</sub> surface. The function of the orientation of adsorbed dipoles of water and CH<sub>3</sub>OH, CHBr<sub>2</sub>, NaOH, and NH<sub>3</sub> molecules has indicated that the charge corresponding to maximum adsorption on B<sub>7</sub>N<sub>6</sub> nanosheet does not stay fixed but differs within rather wide limits depending on the polarity of adsorbates. This affirms the significance of the interaction of adsorbed organic dipoles with the layer field in the adsorption of organic materials on the B<sub>7</sub>N<sub>6</sub> surface.

For calculating the adsorption energy, the total energy of the CH<sub>3</sub>OH, CHBr<sub>2</sub>, NaOH, NH<sub>3</sub> molecules, and B<sub>7</sub>N<sub>6</sub> surface should be computed. As shown in Scheme 1, a graphitic-like

layer of  $B_7N_6$  surface with a length of 25 Å and a bond length of 1.95 Å has been built. Then, it has been tailored the spin-polarized DFT calculation with "ONIOM" model [69] accompanying the same force and energy convergence accuracy to the adsorption systems, with CAM-B3LYP [70] functional and with 6-311+G (d,p) [71] basis set for hydrogen, carbon, nitrogen, oxygen, bromine and LANL2DZ for boron in the adsorption site for the first layer (high level). The second layer (medium level) has been considered on some boron and nitrogen atoms of the  $B_7N_6$  nanosheet in the adsorption site due to semi-empirical methods. The third layer (low level) has been saved on the remaining boron and nitrogen atoms of  $B_7N_6$  nanosheet with molecular mechanic force fields (Scheme 2) [69] as formula:

$$E_{\text{ONIOM}} = E_{1\text{st}} + E_{2\text{nd}} + E_{3\text{rd}} \quad (2)$$



**Scheme 2.** The mechanism of the "Langmuir" adsorption of  $CH_3OH$ ,  $CHBr_2$ ,  $NaOH$ , and  $NH_3$  molecules onto  $B_7N_6$  nanosheet based on optimized coordination towards formation of  $CH_3O-B_7N_6$ ,  $CBr_2-B_7N_6$ ,  $OH-B_7N_6$ , and  $NH_2-B_7N_6$  complexes, respectively.

To determine the most sensitive structure of the  $B_7N_6$  nanosheet as a selective sensor for detecting gas molecules of  $CH_3OH$ ,  $CHBr_2$ ,  $NaOH$ , and  $NH_3$ , the binding energy of each system has been calculated. Therefore, we have found that the priority for selecting the surface binding of O-atom of the  $CH_3O-B_7N_6$  and  $OH-B_7N_6$ , N-atom of  $NH_2$ ,  $B_7N_6$ , and C-atom of  $CBr_2-B_7N_6$  complexes in the adsorption site can be impacted by the existence of close atoms in the  $B_7N_6$  surface. The simulated distribution functions of  $CH_3O-B_7N_6$ ,  $CBr_2-B_7N_6$ ,  $OH-B_7N_6$  and  $NH_2-B_7N_6$  complexes have illustrated that the created clusters lead to the bond lengths of  $O \rightarrow B$  in  $CH_3O-B_7N_6$  (1.55 Å),  $O \rightarrow B$  in  $OH-B_7N_6$  (1.53 Å),  $N \rightarrow B$  in  $NH_2-B_7N_6$  (1.57 Å),  $C \rightarrow B$  in  $CBr_2-B_7N_6$  (1.59 Å) (Scheme 2).

### 3. Results and Discussion

In this research article, boron nitride ( $B_7N_6$ ) nanosheet has been investigated as an efficient surface because of its structural selectivity for the adsorption of water pollutants, including  $CH_3OH$ ,  $CHBr_2$ ,  $NaOH$ , and  $NH_3$  molecules.

These experiments have been accomplished using spectroscopy analysis through some physical and chemical properties of optimized structures of initial compounds and products through the Langmuir adsorption mechanism.

### 3.1. PDOS and electronic analysis.

The electronic structures of CH<sub>3</sub>OH, CHBr<sub>2</sub>, NaOH, and NH<sub>3</sub> adsorbed on the B<sub>7</sub>N<sub>6</sub> nanosheet have been analyzed to simplify subsequent discussion for interfacial electronic properties using CAM-B3LYP/ LANL2DZ, 6-311+G (d,p) basis sets. The graph of partial DOS (PDOS) has illustrated that the *p* states of the adsorption of N<sup>-</sup>, O<sup>-</sup>, and C<sup>-</sup> on the B<sub>7</sub>N<sub>6</sub> nanosheet are dominant through the conduction band (Figure 1a-d). Moreover, the existence of covalent features for these complexes has exhibited the same energy amount and figure of the PDOS for the *p* orbitals of N, O, C, and *d* orbitals of Br (Figure 1a-d).

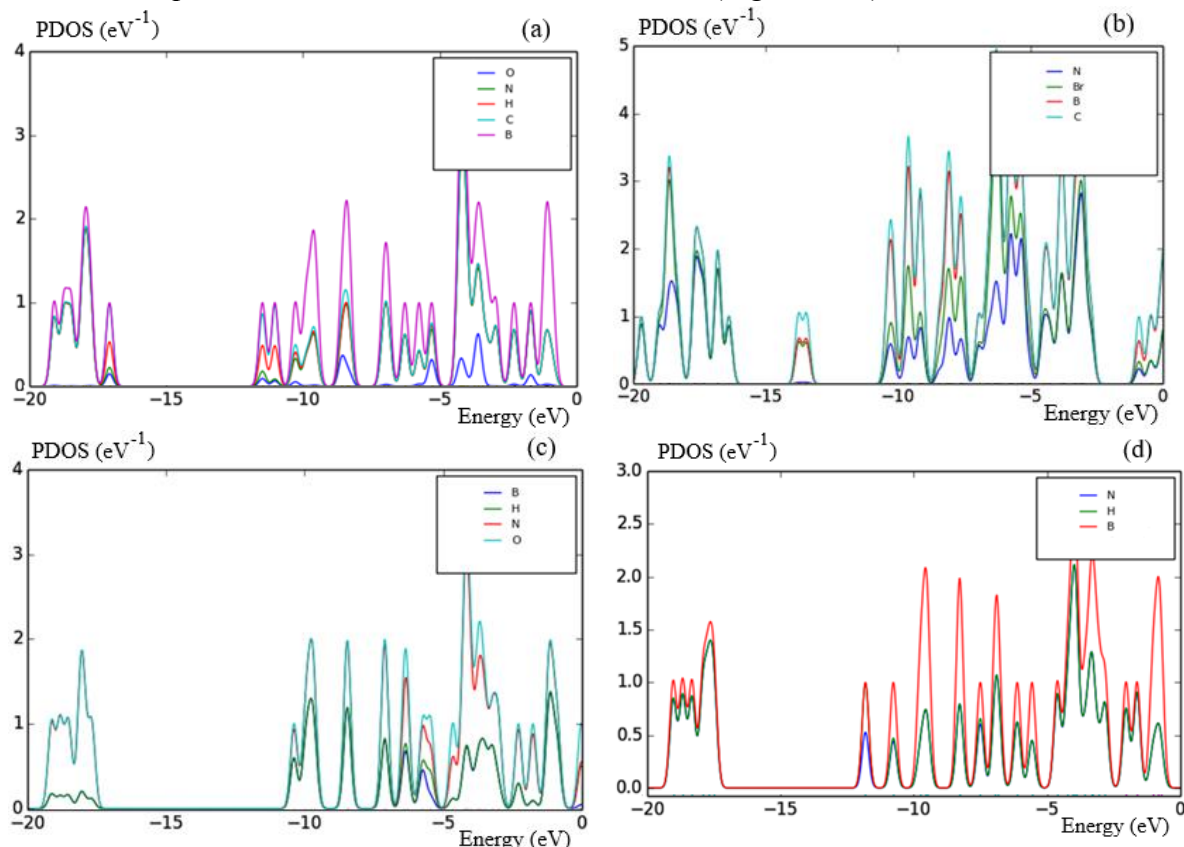


**Figure 1.** PDOS adsorption of CH<sub>3</sub>OH, CHBr<sub>2</sub>, NaOH and NH<sub>3</sub> molecules onto B<sub>7</sub>N<sub>6</sub> nanosheet towards formation of (a) CH<sub>3</sub>O<sup>-</sup> B<sub>7</sub>N<sub>6</sub>; (b) CBr<sub>2</sub><sup>-</sup> B<sub>7</sub>N<sub>6</sub>; (c) OH<sup>-</sup> B<sub>7</sub>N<sub>6</sub>; (d) NH<sub>2</sub><sup>-</sup> B<sub>7</sub>N<sub>6</sub>, respectively.

Figure 1(a-d) shows that the CH<sub>3</sub>O<sup>-</sup>, CBr<sub>2</sub><sup>-</sup>, OH<sup>-</sup>, and NH<sub>2</sub><sup>-</sup> states of CH<sub>3</sub>O<sup>-</sup> B<sub>7</sub>N<sub>6</sub>, CHBr<sub>2</sub><sup>-</sup> B<sub>7</sub>N<sub>6</sub>, OH<sup>-</sup> B<sub>7</sub>N<sub>6</sub>, and NH<sub>2</sub><sup>-</sup> B<sub>7</sub>N<sub>6</sub> nanosheets, respectively, have more contribution at the middle of the conduction band between -5eV to -10eV. Contribution of boron, carbon, and nitrogen states are expanded and close together, but oxygen states have minor contributions in the CH<sub>3</sub>O<sup>-</sup> B<sub>7</sub>N<sub>6</sub> sheet (Figure 1a). In the CHBr<sub>2</sub><sup>-</sup> B<sub>7</sub>N<sub>6</sub> sheet, contributions of nitrogen and oxygen states are expanded and close together, but nitrogen and bromine states have minor contributions (Figure 1b). In the OH<sup>-</sup> B<sub>7</sub>N<sub>6</sub> sheet, contributions of boron and carbon states are expanded and close together, but hydrogen and boron states have minor contributions (Figure 1c). In addition, in the NH<sub>2</sub><sup>-</sup> B<sub>7</sub>N<sub>6</sub> sheet, contributions of hydrogen and boron states are expanded and close together, but nitrogen states have minor contributions (Figure 1d).

The results were also approved by the partial electron density (PDOS), which has shown a certain charge association between the B<sub>7</sub>N<sub>6</sub> nanosheet and water pollutant molecules of CH<sub>3</sub>OH, CHBr<sub>2</sub>, NaOH, and NH<sub>3</sub>.

### 3.2. Nuclear quadrupole resonance (NQR) analysis.

In this research, the calculated "nuclear quadrupole resonance" or "NQR" specifications extract form electrostatic properties have been calculated for CH<sub>3</sub>OH, CHBr<sub>2</sub>, NaOH and NH<sub>3</sub> molecules adsorbed on the B<sub>7</sub>N<sub>6</sub> nanosheet towards formation CH<sub>3</sub>O–B<sub>7</sub>N<sub>6</sub>, CBr<sub>2</sub>–B<sub>7</sub>N<sub>6</sub>, OH–B<sub>7</sub>N<sub>6</sub> and NH<sub>2</sub>–B<sub>7</sub>N<sub>6</sub> which is accord to the results of the "nuclear quadrupole moment", a trait of the nucleus, and the "electric field gradient" or "EFG" in the neighborhood of the nucleus.

As the "EFG" at the citation of the nucleus in CH<sub>3</sub>OH, CHBr<sub>2</sub>, NaOH, and NH<sub>3</sub> is allocated by the valence electrons twisted in the attachment with close nuclei of B<sub>7</sub>N<sub>6</sub> nanosheet, the "NQR" frequency at which transitions occur is particular for (CH<sub>3</sub>OH, CHBr<sub>2</sub>, NaOH, and NH<sub>3</sub>) @ B<sub>7</sub>N<sub>6</sub> complex (Table 1).

In "NMR", nuclei with  $spin \geq 1/2$  have a magnetic dipole moment so that their energies are split by a magnetic field, permitting resonance absorption of energy dependent on the "Larmor frequency";  $\omega_L = \gamma B$ , where  $\gamma$  is the gyromagnetic ratio and  $B$  is the magnetic field external to the nucleus. In "NQR", nuclei with  $spin \geq 1$ , there is an electric quadrupole moment which is accompanied by "non-spherical" nuclear charge diffusions. So, the nuclear charge diffusion is extracted from that of a sphere as the oblate or prolate form of the nucleus [72,73].

"NQR" is a straight frame of the interaction of the "quadrupole moment" with the "EFG", which is produced by the electronic structure of its ambiance. Therefore, the "NQR" transition frequencies are symmetric to the electric quadrupole moment of the nucleus and a measurement of the strength of the local "EFG":  $\omega \sim \frac{e^2 Qq}{h} = C_q$ , where  $q$  is dependent on the biggest fundamental portion of the "EFG" tensor at the nucleus, and  $C_q$  is a quadrupole coupling constant parameter [72,73].

The "NQR" method is related to the multipole expansion in "Cartesian coordinates" as in equation (11):

$$V(r) = V(0) + \left[ \left( \frac{\partial V}{\partial x_i} \right) \Big|_0 \cdot x_i \right] + \frac{1}{2} \left[ \left( \frac{\partial^2 V}{\partial x_i \partial x_j} \right) \Big|_0 \cdot x_i x_j \right] \quad (3)$$

After that, a simplification of the equation (11), there are only the second derivatives related to the identical variable for the "potential energy" [72, 73]:

$$U = -\frac{1}{2} \int_{\mathcal{D}} d^3 r \rho_r \left[ \left( \frac{\partial^2 V}{\partial x_i^2} \right) \Big|_0 \cdot x_i^2 \right] = -\frac{1}{2} \int_{\mathcal{D}} d^3 r \rho_r \left[ \left( \frac{\partial E_i}{\partial x_i} \right) \Big|_0 \cdot x_i^2 \right] = -\frac{1}{2} \left( \frac{\partial E_i}{\partial x_i} \right) \Big|_0 \cdot \int_{\mathcal{D}} d^3 r [\rho(r) \cdot x_i^2] \quad (4)$$

There are two parameters which must be obtained from "NQR" experiments: the "quadrupole coupling constant",  $\chi$ , and "asymmetry parameter" of the "EFG" tensor,  $\eta$ :

$$\chi = \frac{e^2 Q q_{zz}}{h} \quad (5)$$

$$\eta = \frac{q_{xx} - q_{yy}}{q_{zz}} \quad (6)$$

where  $q_{ii}$  are ingredients of the "EFG" tensor at the quadrupole nucleus determined in the "EFG" principal axes system,  $Q$  the "nuclear quadrupole moment",  $e$  the "proton charge", and  $h$  is the "Planck's constant" [74].

In this research work, the "electric potential" as the quantity of work energy through carrying over the electric charge from one position to another position in the essence of electric

field has been evaluated for CH<sub>3</sub>O–B<sub>7</sub>N<sub>6</sub>, CBr<sub>2</sub>– B<sub>7</sub>N<sub>6</sub>, OH– B<sub>7</sub>N<sub>6</sub> and NH<sub>2</sub>– B<sub>7</sub>N<sub>6</sub> complexes using "CAM-B3LYP/EPR-III, LANL2DZ, 6-31+G(d,p)" level of theory (Table 1).

The "electric potential" via "J·C<sup>-1</sup>" is a continuous function in lieu of being generated by a perfect point charge, has  $\frac{1}{r}$  potential:  $V_E = \frac{1}{4\pi\epsilon_0} \frac{Q}{r}$ , where  $Q$  «measured in coulombs» is the point charge,  $r$  is the interval from the charge, and  $\epsilon_0$  is the "permittivity of vacuum".

As the electric potential for a system of point charges is similar to the sum of the point charges' individual potentials, the computations are carried out easily on the basis of the total of potential fields, which are scalar, in lieu of the total of the electric fields, which are vector and much more difficult to compute than the potential field parameter. Therefore,  $V_E(r) = \frac{1}{4\pi\epsilon_0} \sum_i \frac{q_i}{|r-r_i|}$ , where  $r$  is a point at which the potential is evaluated,  $r_i$  is a point at which the charge is  $\neq 0$ , and  $q_i$  is the charge at the point  $r_i$ . Finally, the potential of a continuous charge diffusion  $\rho(r)$  is explored:  $V_E(r) = \frac{1}{4\pi\epsilon_0} \int_R \frac{\rho(r')}{|r-r'|} d^3r'$ , where  $R$  is a set containing all the points at which the charge density is  $\neq 0$ ,  $r'$  is a point inside  $R$ , and  $\rho(r')$  is the charge density at the point  $r'$  [75].

**Table 1.** The electric potential (E<sub>p</sub>/a.u.) and Bader charge (Q/e) for elements of H, B, C, N, O, and Br of CH<sub>3</sub>O–B<sub>7</sub>N<sub>6</sub>, CBr<sub>2</sub>–B<sub>7</sub>N<sub>6</sub>, OH–B<sub>7</sub>N<sub>6</sub>, and NH<sub>2</sub>–B<sub>7</sub>N<sub>6</sub> complexes by CAM-B3LYP/EPR-III,6-31+G(d,p) calculation extracted from "NQR" method.

CH <sub>3</sub> O–B <sub>7</sub> N <sub>6</sub>			CBr <sub>2</sub> –B <sub>7</sub> N <sub>6</sub>			OH– B <sub>7</sub> N <sub>6</sub>			NH <sub>2</sub> – B <sub>7</sub> N <sub>6</sub>		
Atom	Q	E <sub>p</sub>	Atom	Q	E <sub>p</sub>	Atom	Q	E <sub>p</sub>	Atom	Q	E <sub>p</sub>
C1	-0.1524	-14.5195	Br1	0.0804	-174.404	O1	-0.087	-22.0371	N1	-0.3964	-18.1251
O2	-0.1670	-22.0359	C2	-0.1406	-14.57	B2	0.1776	-11.4396	H2	0.1737	-1.06079
B3	0.1686	-11.4389	B3	0.1904	-11.4389	N3	-0.2607	-18.1391	H3	0.1730	-1.0655
N4	-0.2719	-18.1469	N4	-0.3248	-18.2041	B4	0.1945	-11.4222	B4	0.1707	-11.4469
B5	0.1919	-11.4259	B5	0.1936	-11.4465	B5	0.2154	-11.4149	N5	-0.2643	-18.1466
B6	0.2174	-11.4172	B6	0.1801	-11.443	N6	-0.1771	-18.1825	B6	0.1883	-11.4302
N7	-0.1779	-18.1857	N7	-0.1948	-18.2133	B7	0.1860	-11.4406	B7	0.2020	-11.4234
B8	0.1853	-11.4397	B8	0.2162	-11.4133	N8	-0.1909	-18.2002	N8	-0.1762	-18.1852
N9	-0.1883	-18.1975	N9	-0.1874	-18.198	N9	-0.2508	-18.1347	B9	0.1737	-11.45
N10	-0.2596	-18.1418	N10	-0.2929	-18.1624	B10	0.2683	-11.3214	N10	-0.1995	-18.2097
B11	0.2793	-11.324	B11	0.2632	-11.3376	B11	0.2142	-11.4135	N11	-0.2485	-18.1383
B12	0.2157	-11.4132	B12	0.2045	-11.4264	N12	-0.2980	-18.1611	B12	0.3322	-11.3063
N13	-0.2922	-18.1617	N13	-0.3228	-18.2006	B13	0.1936	-11.4239	B13	0.1928	-11.4314
B14	-0.1979	-11.4223	B14	0.2230	-11.411	N14	-0.1738	-18.1796	N14	-0.3014	-18.1699
N15	-0.1731	-18.18	N15	-0.1684	-18.1793	H15	-0.0113	-1.19619	B15	0.1701	-11.4436
H16	0.0827	-1.13763	Br16	0.0802	-174.409				N16	-0.1903	-18.1985
H17	0.0753	-1.13664									
H18	0.0681	-1.15514									

Furthermore, in Figure 2(a-d), it has been sketched the "electric potential" of nuclear quadrupole resonance for some atoms of hydrogen, boron, carbon, nitrogen, oxygen and bromine in the adsorption process of CH<sub>3</sub>OH, CHBr<sub>2</sub>, NaOH and NH<sub>3</sub> molecules adsorbed on the B<sub>7</sub>N<sub>6</sub> nanosheet which have been calculated by "CAM-B3LYP/EPR-III, 6-311+G (d,p), LANL2DZ".

In Figure 2 (a-d), the changes of electric potential for hydrogen, boron, carbon, nitrogen, oxygen, and bromine are shown in the active site of Langmuir adsorption. In fact, it has been observed the effect of the binding between C, N, and O with boron in the B<sub>7</sub>N<sub>6</sub> nanosheet during adsorbing CH<sub>3</sub>OH, CHBr<sub>2</sub>, NaOH and NH<sub>3</sub> molecules through resulted electric potential using NQR analysis with relation coefficients of R<sup>2</sup>= 0.9423 for CH<sub>3</sub>O– B<sub>7</sub>N<sub>6</sub>

(Figure 2a),  $R^2= 0.9525$  for  $\text{CBr}_2\text{- B}_7\text{N}_6$  (Figure 2b),  $R^2= 0.9804$  for  $\text{OH- B}_7\text{N}_6$  (Figure 2c), and  $R^2= 0.9533$  for  $\text{NH}_2\text{- B}_7\text{N}_6$  (Figure 2d).

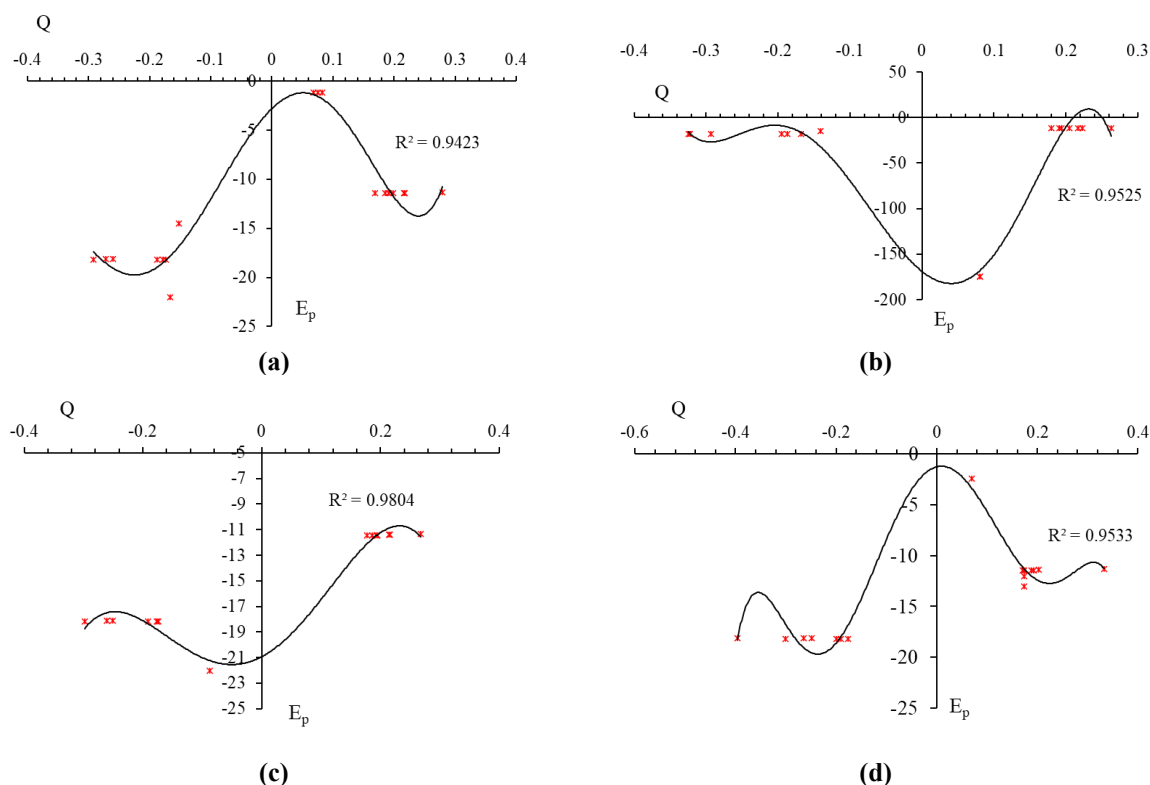


**Figure 2.** The electric potential versus Bader charge through NQR calculation for adsorption clusters of (a)  $\text{CH}_3\text{O- B}_7\text{N}_6$ ; (b)  $\text{CBr}_2\text{- B}_7\text{N}_6$ ; (c)  $\text{OH- B}_7\text{N}_6$ ; (d)  $\text{NH}_2\text{- B}_7\text{N}_6$  using CAM-B3LYP/EPR-III, LANL2DZ, 6-31+G(d,p).

It's obvious that the capability of  $\text{B}_7\text{N}_6$  nanosheet for detecting  $\text{CH}_3\text{OH}$ ,  $\text{CHBr}_2$ ,  $\text{NaOH}$ , and  $\text{NH}_3$  molecules is fluctuated by their selectivity and sensitivity, which can represent the efficiency of these surfaces as promising sensors.

### 3.3. "NMR" spectroscopy.

Isotropic ( $\sigma_{\text{iso}}$ ) and anisotropy ( $\sigma_{\text{aniso}}$ ) shielding tensors of "NMR" spectroscopy for certain atoms in the active site of  $\text{CH}_3\text{OH}$ ,  $\text{CHBr}_2$ ,  $\text{NaOH}$ , and  $\text{NH}_3$  adsorbed on the  $\text{B}_7\text{N}_6$  nanosheet through the formation of the binding between gas molecules and solid surfaces have been calculated using Gaussian 16, Revision C.01, and reported in Table 2 [50].

**Table 2.** Data of "NMR" shielding tensors for selected atoms of  $\text{CH}_3\text{OH}$ ,  $\text{CHBr}_2$ ,  $\text{NaOH}$ , and  $\text{NH}_3$  through adsorption on  $\text{B}_7\text{N}_6$  nanosheet using CAM-B3LYP/EPR-III, 6-311+G (d,p) calculation.

$\text{CH}_3\text{O- B}_7\text{N}_6$			$\text{CBr}_2\text{- B}_7\text{N}_6$			$\text{OH- B}_7\text{N}_6$			$\text{NH}_2\text{- B}_7\text{N}_6$		
Atom	$\sigma_{\text{iso}}$	$\sigma_{\text{aniso}}$	Atom	$\sigma_{\text{iso}}$	$\sigma_{\text{aniso}}$	Atom	$\sigma_{\text{iso}}$	$\sigma_{\text{aniso}}$	Atom	$\sigma_{\text{iso}}$	$\sigma_{\text{aniso}}$
C1	207.4900	229.8084	Br1	2255.6038	448.6099	O1	4188.7985	19001.3542	N1	397.5544	1522.0783
O2	2571.7358	5404.2611	C2	79.1939	264.6245	B2	1711.2615	3150.3904	H2	45.2678	85.8620
B3	1887.2958	4827.1381	B3	42.0204	57.8614	N3	5221.2659	16311.0488	H3	47.9762	86.4201
N4	7888.2732	26535.9295	N4	143.3403	134.8370	B4	452.2991	1628.2843	B4	1152.1291	3921.2721
B5	631.2083	2792.3878	B5	36.0191	43.5880	B5	861.3538	3416.7600	N5	1955.0602	11129.1217
B6	1730.2348	4161.3618	B6	47.3299	73.6073	N6	10146.9927	50000.0792	B6	695.8646	1981.2237
N7	7582.0326	60137.9910	N7	511.7273	580.4868	B7	688.4710	5200.7121	B7	820.3862	2506.3503
B8	267.9068	8069.0999	B8	65.1754	118.3058	N8	11461.9126	43429.9639	N8	3210.5811	24161.4011
N9	20673.2800	77041.4503	N9	519.3833	544.7120	N9	1060.4445	7260.2782	B9	1035.5334	4329.1213
N10	719.6112	10666.3043	N10	131.7461	174.6893	B10	158.7282	348.4470	N10	10325.7680	20459.1621
B11	174.9055	545.2617	B11	30.1945	51.7908	B11	669.0245	4104.9100	N11	639.7713	4065.1118
B12	1262.5805	6875.7306	B12	18.4989	54.0664	N12	338.0289	3330.8232	B12	31.5242	385.1119
N13	1439.6410	7609.1711	N13	185.9407	247.9779	B13	451.9133	2065.4295	B13	53.4323	627.1198
B14	1009.6465	3656.9631	B14	28.5714	49.5475	N14	14659.7719	54547.1808	N14	108.6987	5495.2593

CH <sub>3</sub> O- B <sub>7</sub> N <sub>6</sub>			CBr <sub>2</sub> - B <sub>7</sub> N <sub>6</sub>			OH- B <sub>7</sub> N <sub>6</sub>			NH <sub>2</sub> - B <sub>7</sub> N <sub>6</sub>		
Atom	$\sigma_{iso}$	$\sigma_{aniso}$	Atom	$\sigma_{iso}$	$\sigma_{aniso}$	Atom	$\sigma_{iso}$	$\sigma_{aniso}$	Atom	$\sigma_{iso}$	$\sigma_{aniso}$
N15	22798.1457	85933.4663	N15	316.1337	195.8486	H15	15.4447	90.5114	B15	82.1396	743.1337
H16	24.8998	81.1985	Br16	2188.9136	599.4625				N16	6146.7100	8153.3246
H17	44.9274	128.6231									
H18	11.1081	62.6904									

In Table 2, "NMR" data have reported the notable amounts for CH<sub>3</sub>OH, CHBr<sub>2</sub>, NaOH, and NH<sub>3</sub>, which have been doped on the B<sub>7</sub>N<sub>6</sub> nanosheet.

In fact, the adsorption of CH<sub>3</sub>OH, CHBr<sub>2</sub>, NaOH, and NH<sub>3</sub> introduces spin polarization on the B<sub>7</sub>N<sub>6</sub> nanosheet, which indicates that this surface might be applied as magnetic carbon, nitrogen, and oxygen detectors. In fact, it is revealed that the "isotropic" and "anisotropy" shielding augment with the occupancy in CH<sub>3</sub>OH, CHBr<sub>2</sub>, NaOH and NH<sub>3</sub> penetrated by "C-, N-, O-atoms" in CH<sub>3</sub>O- B<sub>7</sub>N<sub>6</sub> (O→B), CBr<sub>2</sub>- B<sub>7</sub>N<sub>6</sub> (C→B), OH- B<sub>7</sub>N<sub>6</sub> (O→B) and NH<sub>2</sub>- B<sub>7</sub>N<sub>6</sub> (N→B) (Figure 3a-d).

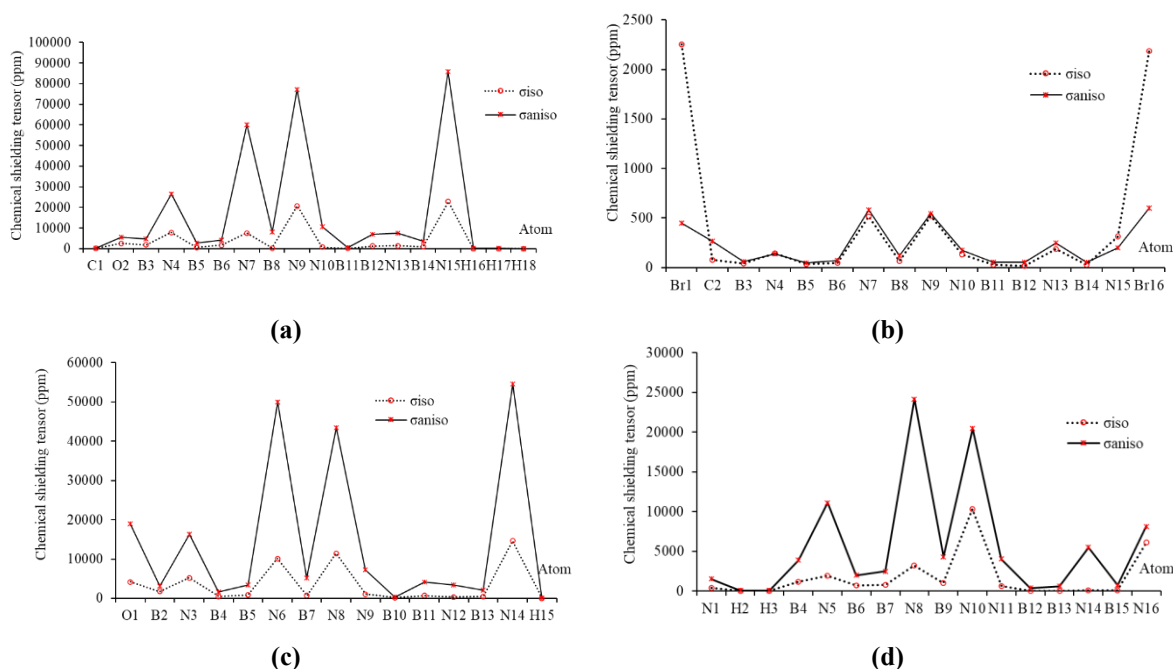


**Figure 3.** "NMR" adsorbing of CH<sub>3</sub>OH, CHBr<sub>2</sub>, NaOH and NH<sub>3</sub> through adsorption on B<sub>7</sub>N<sub>6</sub> nanosheet through production of (a) CH<sub>3</sub>O- B<sub>7</sub>N<sub>6</sub>; (b) CBr<sub>2</sub>- B<sub>7</sub>N<sub>6</sub>; (c) OH- B<sub>7</sub>N<sub>6</sub>; (d)NH<sub>2</sub>- B<sub>7</sub>N<sub>6</sub> using CAM-B3LYP/EPR-III, LANL2DZ,6-31+G(d,p).

The resulted graphs of "NMR" data in Figure 3 (a-d) have shown approximately the identical chemical shielding behavior of isotropic and anisotropy factors for CH<sub>3</sub>O- B<sub>7</sub>N<sub>6</sub>, OH- B<sub>7</sub>N<sub>6</sub> and NH<sub>2</sub>- B<sub>7</sub>N<sub>6</sub> with several sharp peaks related to nitrogen atoms involving the adsorption site including (N7, N9, N15) (Figure 3a), (N6, N8, N14) (Figure 3c), and (N5, N8, N10) (Figure3d).

However, has been shown that CBr<sub>2</sub>- B<sub>7</sub>N<sub>6</sub> has two sharp peaks related to boron and carbon atoms involving the adsorption site, including (B16 and C2) (Figure 3b).

Although in the NMR spectroscopy, the remarkable peaks around carbon, nitrogen, oxygen, and bromine atoms through the adsorption procedure of CH<sub>3</sub>OH, CHBr<sub>2</sub>, NaOH, and NH<sub>3</sub> on the B<sub>7</sub>N<sub>6</sub> nanosheet, there are some fluctuations in the chemical shielding behaviors of isotropic and anisotropic attributes.

### 3.4. "IR" insight and thermodynamic analysis.

In this part, the stability of complexes including water pollutants of CH<sub>3</sub>OH, CHBr<sub>2</sub>, NaOH, and NH<sub>3</sub> adsorbed on the boron nitride (B<sub>7</sub>N<sub>6</sub>) nanosheet has been investigated through thermodynamic properties, which define the reactions that CH<sub>3</sub>OH, CHBr<sub>2</sub>, NaOH, and NH<sub>3</sub> endure in the boron coordination sphere. Concerning the adsorption process, the thermodynamic characters were evaluated for CH<sub>3</sub>OH, CHBr<sub>2</sub>, NaOH, and NH<sub>3</sub> and complexes of CH<sub>3</sub>O– B<sub>7</sub>N<sub>6</sub>, CBr<sub>2</sub>– B<sub>7</sub>N<sub>6</sub>, OH– B<sub>7</sub>N<sub>6</sub>, and NH<sub>2</sub>– B<sub>7</sub>N<sub>6</sub> on the surface of B<sub>7</sub>N<sub>6</sub> nanosheet as the water pollutant detectors which can be applicable as the selective sensors for these compounds removal (Table 3).

**Table 3.** The thermodynamic character of CH<sub>3</sub>OH, CHBr<sub>2</sub>, NaOH, and NH<sub>3</sub> adsorbed on the B<sub>7</sub>N<sub>6</sub> nanosheet as the selective water pollutant sensors.

Compound	$\Delta H^\circ \times 10^{-4}$ (kcal/mol)	$\Delta G^\circ \times 10^{-4}$ (kcal/mol)	S <sup>o</sup> (cal/K.mol)	Dipole moment (Debye)
CH <sub>3</sub> OH	-7.1568	-7.1584	55.576	1.3748
CHBr <sub>2</sub>	-321.9162	-321.9183	71.878	0.8932
NaOH	-14.7376	-14.7393	56.923	6.6903
NH <sub>3</sub>	-3.4958	-3.4973	48.843	1.6650
B <sub>7</sub> N <sub>6</sub> nanosheet	-31.0214	-31.0238	103.077	0.4110
CH <sub>3</sub> O- B <sub>7</sub> N <sub>6</sub>	-38.1324	-38.1355	104.117	1.3507
CBr <sub>2</sub> - B <sub>7</sub> N <sub>6</sub>	-352.9039	-352.9075	120.009	2.2734
OH- B <sub>7</sub> N <sub>6</sub>	-35.6875	-35.6907	106.940	1.7390
NH <sub>2</sub> - B <sub>7</sub> N <sub>6</sub>	-34.4705	-34.4736	104.137	1.0754

Furthermore, the "IR" spectra for the adsorption of CH<sub>3</sub>OH, CHBr<sub>2</sub>, NaOH, and NH<sub>3</sub> on the surface of the boron nitride (B<sub>7</sub>N<sub>6</sub>) nanosheet have been reported in Figure 4.

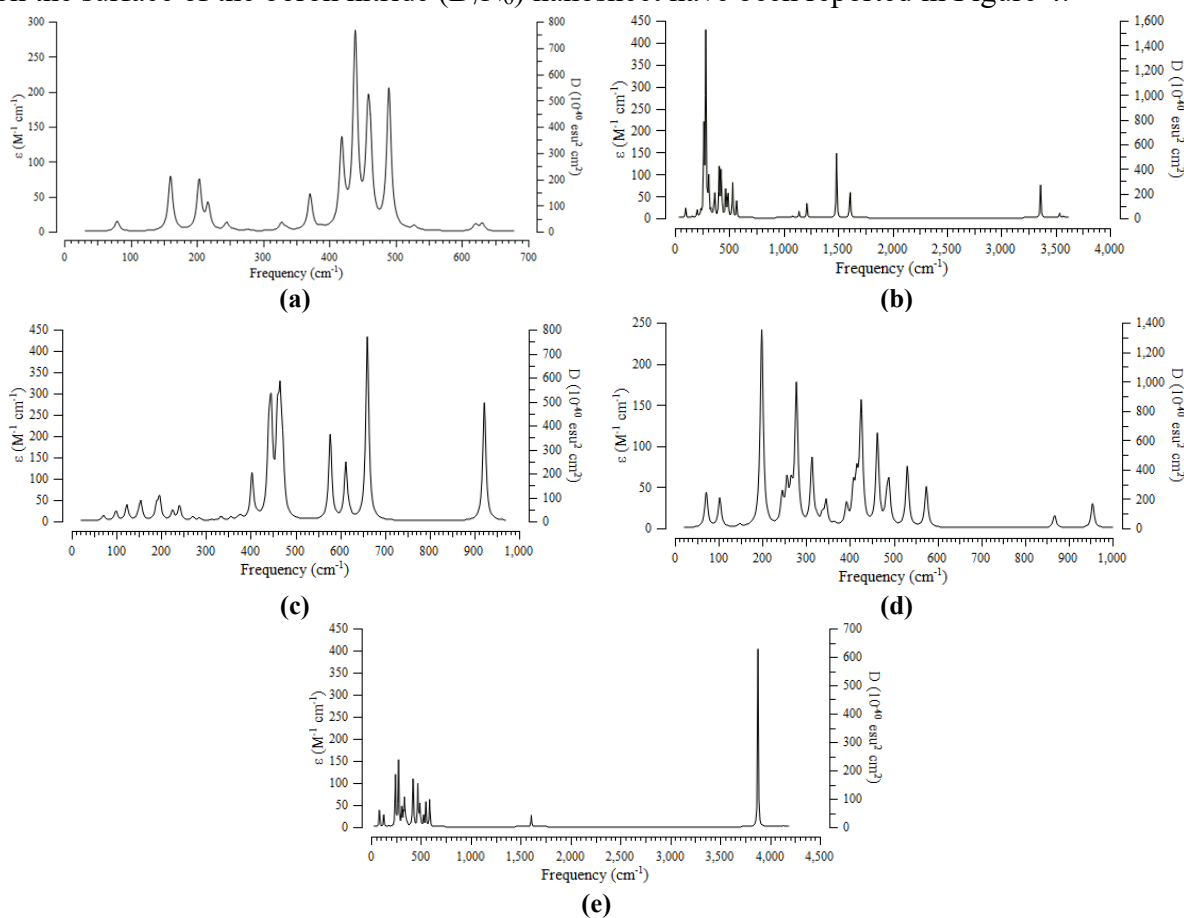


**Figure 4.** The frequency ( $cm^{-1}$ ) changes through the "IR" spectra for (a) B<sub>7</sub>N<sub>6</sub> nanosheet; (b) CH<sub>3</sub>O- B<sub>7</sub>N<sub>6</sub>; (c) CBr<sub>2</sub>- B<sub>7</sub>N<sub>6</sub>; (d) OH- B<sub>7</sub>N<sub>6</sub>; (e) NH<sub>2</sub>- B<sub>7</sub>N<sub>6</sub> complexes.

The graphs of Figure 4 (a) have been observed in the frequency range between 100 cm<sup>-1</sup> and 700 cm<sup>-1</sup> for the B<sub>7</sub>N<sub>6</sub> nanosheet. Figure 4 (b) shows the frequency range between 100 cm<sup>-1</sup> and 3500 cm<sup>-1</sup> for the CH<sub>3</sub>O– B<sub>7</sub>N<sub>6</sub> complex with a sharp peak around 250 cm<sup>-1</sup>. Figure 4 (c and d) has a similar fluctuation of frequency between 100 cm<sup>-1</sup>-1000 cm<sup>-1</sup> for CBr<sub>2</sub>– B<sub>7</sub>N<sub>6</sub> Figure 4 (c) with several sharp peaks around 450 cm<sup>-1</sup>, 650 cm<sup>-1</sup>, 950 cm<sup>-1</sup>, and for OH– B<sub>7</sub>N<sub>6</sub> Figure 4 (d) with several sharp peaks around 200 cm<sup>-1</sup>, 270 cm<sup>-1</sup>, 420 cm<sup>-1</sup>, respectively. Moreover, NH<sub>2</sub>– B<sub>7</sub>N<sub>6</sub> has remarked a considerable frequency peak about 3850 cm<sup>-1</sup>, Figure 4 (e).

In addition, the high amounts of the "Langmuir" adsorption isotherm graphs based on relative adsorption energy ( $\Delta G^{\circ}_{\text{ads}}$ ) have been evaluated for interactions between CH<sub>3</sub>OH, CHBr<sub>2</sub>, NaOH, and NH<sub>3</sub> on the surface of B<sub>7</sub>N<sub>6</sub> nanosheet with R<sup>2</sup> = 0.873 (Figure 5).

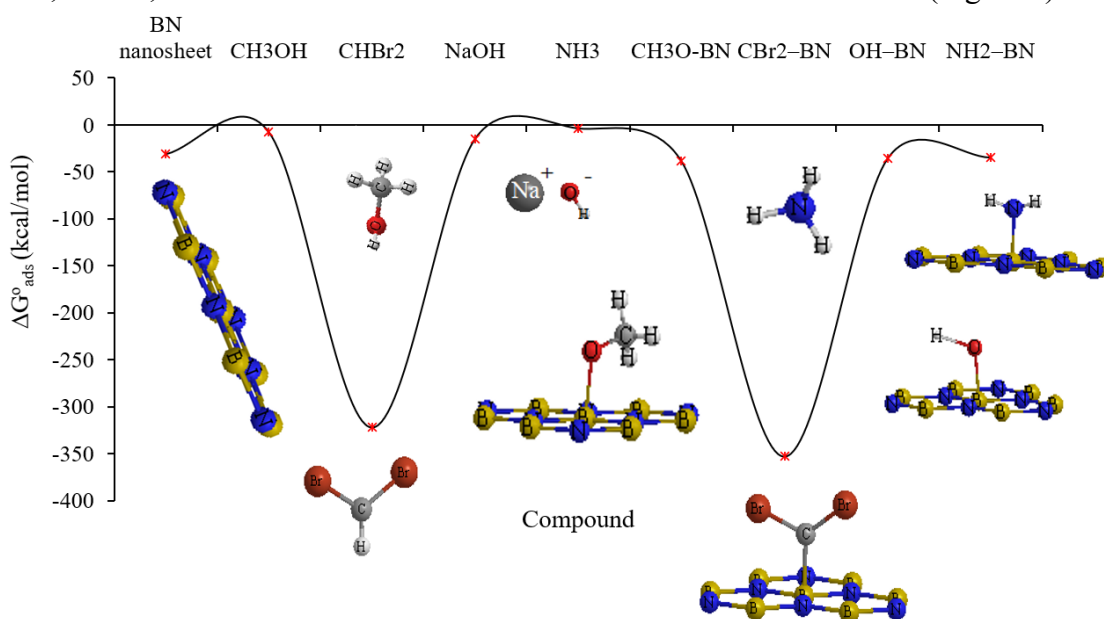


**Figure 5.** The alterations of adsorption Gibbs free energy ( $\Delta G^{\circ}_{\text{ads}}$ ) CH<sub>3</sub>OH, CHBr<sub>2</sub>, NaOH and NH<sub>3</sub> adsorbed on the B<sub>7</sub>N<sub>6</sub> nanosheet and formation of CH<sub>3</sub>O– B<sub>7</sub>N<sub>6</sub>, CBr<sub>2</sub>– B<sub>7</sub>N<sub>6</sub>, OH– B<sub>7</sub>N<sub>6</sub> and NH<sub>2</sub>– B<sub>7</sub>N<sub>6</sub> complexes.

The adsorptive capacity of CH<sub>3</sub>OH, CHBr<sub>2</sub>, NaOH, and NH<sub>3</sub> on the surface of B<sub>7</sub>N<sub>6</sub> nanosheet is approved by the  $\Delta G^{\circ}_{\text{ads}}$  amounts as follows:

$$\Delta G^{\circ}_{\text{ads}} = \Delta G^{\circ}_{\text{X} \rightarrow \text{B7N6\_NS}} - (\Delta E^{\circ}_{\text{X}} + \Delta E^{\circ}_{\text{B7N6\_NS}}); (\text{X} = \text{CH}_3\text{OH}, \text{CHBr}_2, \text{NaOH}, \text{NH}_3) \quad (7)$$

Table 3 shows that the adsorption of CH<sub>3</sub>OH, CHBr<sub>2</sub>, NaOH, and NH<sub>3</sub> on the surface of B<sub>7</sub>N<sub>6</sub> nanosheet must have both "physical" and "chemical" nature. All the measured relative adsorption energies ( $\Delta G^{\circ}_{\text{ads}}$ ) are almost identical and exhibit the most stable Gibbs free energy for CHBr<sub>2</sub> and CBr<sub>2</sub>– B<sub>7</sub>N<sub>6</sub> (Figure 5). In fact, boron sites in B<sub>7</sub>N<sub>6</sub> nanosheet have higher interaction energy from Van der Waals' forces with the molecules of CH<sub>3</sub>OH, CHBr<sub>2</sub>, NaOH, and NH<sub>3</sub> that can make them highly stable.

Furthermore, the results of Table 3 have indicated that CH<sub>3</sub>OH → B<sub>7</sub>N<sub>6</sub>, CHBr<sub>2</sub> → B<sub>7</sub>N<sub>6</sub>, NaOH → B<sub>7</sub>N<sub>6</sub> and NH<sub>3</sub> → B<sub>7</sub>N<sub>6</sub> complexes have the largest gap of Gibbs free energy adsorption with which defines the changes between Gibbs free energy of initial compounds ( $\Delta G^{\circ}_{\text{CH}_3\text{OH}}, \Delta G^{\circ}_{\text{CHBr}_2}, \Delta G^{\circ}_{\text{NaOH}}, \Delta G^{\circ}_{\text{NH}_3}$ ) and ( $\Delta G^{\circ}_{\text{B7N6\_NS}}$ ) and product compounds ( $\Delta G^{\circ}_{\text{CH}_3\text{O-B7N6}}, \Delta G^{\circ}_{\text{CBr}_2\text{-B7N6}}, \Delta G^{\circ}_{\text{OH-B7N6}}, \Delta G^{\circ}_{\text{NH}_2\text{-B7N6}}$ ) through polarizability. However, the B<sub>7</sub>N<sub>6</sub> nanosheet seems to possess enough efficiency for the adsorption of water pollutants of CH<sub>3</sub>OH,

CHBr<sub>2</sub>, NaOH, and NH<sub>3</sub> through charge transfer from carbon, nitrogen, and oxygen to the boron element due to intra-atomic and interatomic interactions.

#### 4. Conclusions

The adsorption performance and mechanism of B<sub>7</sub>N<sub>6</sub> nanosheet for CH<sub>3</sub>OH, CHBr<sub>2</sub>, NaOH, and NH<sub>3</sub> molecules were investigated. The amounts of changes of charge density have shown a more important charge transfer for B<sub>7</sub>N<sub>6</sub> nanosheet, which acts as the electron acceptor, while organic molecules act as the electron donors through adsorption on the graphitic-like B<sub>7</sub>N<sub>6</sub> surface. It has been assumed that the priority for selecting the surface binding of C-atom of CHBr<sub>2</sub>, N-atom of NH<sub>3</sub>, and O-atom of CH<sub>3</sub>OH & NaOH in adsorption site can be impacted by the existence of close atoms in the B<sub>7</sub>N<sub>6</sub> surface through formation of CH<sub>3</sub>O–B<sub>7</sub>N<sub>6</sub>, CBr<sub>2</sub>–B<sub>7</sub>N<sub>6</sub>, OH–B<sub>7</sub>N<sub>6</sub> and NH<sub>2</sub>–B<sub>7</sub>N<sub>6</sub> complexes. All in all, the boron site in the B<sub>7</sub>N<sub>6</sub> nanosheet has a higher interaction energy from Van der Waals' forces with organic molecules, including CH<sub>3</sub>OH, CHBr<sub>2</sub>, NaOH, and NH<sub>3</sub>, that can make them highly stable. The current work summarizes the possibility of B<sub>7</sub>N<sub>6</sub>-based nanomaterials as adsorbents for the adsorption of some organic contaminants of CH<sub>3</sub>OH, CHBr<sub>2</sub>, NaOH, and NH<sub>3</sub>. The results showed that B<sub>7</sub>N<sub>6</sub>-based nano adsorbents can be a preferable option, presently used or studied for water and wastewater purification.

#### Author Contributions

All authors have read and agreed to the published version of the manuscript.

#### Institutional Review Board Statement

Not applicable.

#### Informed Consent Statement

Not applicable.

#### Data Availability Statement

Not applicable.

#### Funding

This research received no external funding.

#### Acknowledgments

In successfully completing this paper and its research, the author is grateful to Kastamonu University.

#### Conflict of Interest

The author declares no conflict of interest.

#### References

1. Mollaamin, F.; Monajjemi, M. Nanomaterials for Sustainable Energy in Hydrogen-Fuel Cell: Functionalization and Characterization of Carbon Nano-Semiconductors with Silicon, Germanium, Tin or Lead through Density Functional Theory Study. *Russ. J. Phys. Chem. B.* **2024**, *18*, 607–623, <https://doi.org/10.1134/S1990793124020271>.

2. Mollaamin, F.; Monajjemi, M. Doping of Graphene Nanostructure with Iron, Nickel and Zinc as Selective Detector for the Toxic Gas Removal: A Density Functional Theory Study. *C-Journal of Carbon Reseach*. **2023**, *9*, 20, <https://doi.org/10.3390/c9010020>.
3. Zhong, Q.-L.; Chen, Z.; Shen, Q.; Xiong, J.-Q. Occurrence of antibiotics in reclaimed water, and their uptake dynamics, phytotoxicity, and metabolic fate in *Lolium perenne* L. *Sci. Total Environ.* **2023**, *904*, 166975, <https://doi.org/10.1016/j.scitotenv.2023.166975>.
4. Tkaczyk, A.; Mitrowska, K.; Posyniak, A. Synthetic organic dyes as contaminants of the aquatic environment and their implications for ecosystems: A review. *Sci. Total Environ.* **2020**, *717*, 137222, <https://doi.org/10.1016/j.scitotenv.2020.137222>.
5. Mollaamin, F.; Monajjemi, M. Molecular modelling framework of metal-organic clusters for conserving surfaces: Langmuir sorption through the TD-DFT/ONIOM approach. *Mol. Simul.* **2022**, *49*, 365–376, <https://doi.org/10.1080/08927022.2022.2159996>.
6. Vardhan, K.H.; Kumar, P.S.; Panda, R.C. A review on heavy metal pollution, toxicity and remedial measures: Current trends and future perspectives. *J. Mol. Liq.* **2019**, *290*, 111197, <https://doi.org/10.1016/J.MOLLIQ.2019.111197>.
7. Dixit, F.; Dutta, R.; Barbeau, B.; Berube, P.; Mohseni, M. PFAS removal by ion exchange resins: A review. *Chemosphere* **2021**, *272*, 129777, <https://doi.org/10.1016/j.chemosphere.2021.129777>.
8. Kim, S.; Muñoz-Senmache, J.C.; Jun, B.-M.; Park, C.M.; Jang, A.; Yu, M.; Hernández-Maldonado, A.J.; Yoon, Y. A metal organic framework-ultrafiltration hybrid system for removing selected pharmaceuticals and natural organic matter. *Chem. Eng. J.* **2020**, *382*, 122920, <https://doi.org/10.1016/j.cej.2019.122920>.
9. Lacson, C.F.Z.; Lu, M.-C.; Huang, Y.-H. Chemical precipitation at extreme fluoride concentration and potential recovery of CaF<sub>2</sub> particles by fluidized-bed homogenous crystallization process. *Chem. Eng. J.* **2021**, *415*, 128917, <https://doi.org/10.1016/j.cej.2021.128917>.
10. Oladoye, P.O. Natural, low-cost adsorbents for toxic Pb(II) ion sequestration from (waste)water: A state-of-the-art review. *Chemosphere* **2022**, *287*, 132130, <https://doi.org/10.1016/j.chemosphere.2021.132130>.
11. Joseph, L.; Jun, B.-M.; Flora, J.R.V.; Park, C.M.; Yoon, Y. Removal of heavy metals from water sources in the developing world using low-cost materials: A review. *Chemosphere* **2019**, *229*, 142–159, <https://doi.org/10.1016/j.chemosphere.2019.04.198>.
12. Mollaamin, F.; Monajjemi, M. Fractal Dimension on Carbon Nanotube-Polymer Composite Materials Using Percolation Theory. *J. Comput. Theor. Nanosci.* **2012**, *9*, 597–601, <https://doi.org/10.1166/jctn.2012.2067>.
13. Jun, B.-M.; Kim, S.; Kim, Y.; Her, N.; Heo, J.; Han, J.; Jang, M.; Park, C.M.; Yoon, Y. Comprehensive evaluation on removal of lead by graphene oxide and metal organic framework. *Chemosphere* **2019**, *231*, 82–92, <https://doi.org/10.1016/j.chemosphere.2019.05.076>.
14. Jeon, M.; Jun, B.-M.; Kim, S.; Jang, M.; Park, C.M.; Snyder, S.A.; Yoon, Y. A review on MXene-based nanomaterials as adsorbents in aqueous solution. *Chemosphere* **2020**, *261*, 127781, <https://doi.org/10.1016/j.chemosphere.2020.127781>.
15. Ihsanullah, I. Boron nitride-based materials for water purification: Progress and outlook. *Chemosphere* **2021**, *263*, 127970, <https://doi.org/10.1016/j.chemosphere.2020.127970>.
16. Mollaamin, F.; Monajjemi, M. An Architectural Battery Designed by Substituting Lithium with Second Main Group Metals (Be, Mg, Ca/Cathode) and Hybrid Oxide of Fourth Group Ones (Si, Ge, Sn/Anode) Nanomaterials Towards H<sub>2</sub> Adsorption: A Computational Study. *Nanomaterials* **2025**, *15*, 959, <https://doi.org/10.3390/nano15130959>
17. Pu, J.; Zhang, K.; Wang, Z.; Li, C.; Zhu, K.; Yao, Y.; Hong, G. Synthesis and Modification of Boron Nitride Nanomaterials for Electrochemical Energy Storage: From Theory to Application. *Adv. Funct. Mater.* **2021**, *31*, 2106315, <https://doi.org/10.1002/adfm.202106315>.
18. Maestre, C.; Toury, B.; Steyer, P.; Garnier, V.; Journet, C. Hexagonal boron nitride: a review on selfstanding crystals synthesis towards 2D nanosheets. *J. Phys. Mater.* **2021**, *4*, 044018, <https://doi.org/10.1088/2515-7639/ac2b87>.
19. Mollaamin, F. Anchoring of 2D layered materials of Ge<sub>5</sub>Si<sub>5</sub>O<sub>20</sub> for (Li/Na/K)-(Rb/Cs) batteries towards Eco-friendly energy storage. *BMC Chemistry*. **2025**, *19*, 233, <https://doi.org/10.1186/s13065-025-01593-0>.
20. Muñoz, A.D.O.; Escobedo-Morales, A.; Skakerzadeh, E.; Anot, E.C. Effect of homonuclear boron bonds in the adsorption of DNA nucleobases on boron nitride nanosheets. *J. Mol. Liq.* **2021**, *322*, 114951, <https://doi.org/10.1016/j.molliq.2020.114951>.

21. Mollaamin, F.; Monajjemi, M. Perspective of Clean Energy-saving by Semiconducting Quantum Dot Nanomaterials through Photoelectric and Density of States Analysis. *J. Fluoresc.* **2025**, <https://doi.org/10.1007/s10895-025-04207-z>.
22. Mollaamin, F.; Mohammadi, S.; Khalaj, Z.; Monajjemi, M. Computational Modelling of Boron Nitride Nanosheet for Detecting and Trapping of Water Contaminant. *Russ. J. Phys. Chem. B* **2024**, *18*, 67–82, <https://doi.org/10.1134/S1990793124010330>.
23. Murzakhanov, F.F.; Yavkin, B.V.; Mamin, G.V.; Orlinskii, S.B.; Mumdzhi, I.E.; Gracheva, I.N.; Gabbasov, B.F.; Smirnov, A.N.; Davydov, V.Y.; Soltamov, V.A. Creation of Negatively Charged Boron Vacancies in Hexagonal Boron Nitride Crystal by Electron Irradiation and Mechanism of Inhomogeneous Broadening of Boron Vacancy-Related Spin Resonance Lines. *Nanomaterials* **2021**, *11*, 1373, <https://doi.org/10.3390/nano11061373>.
24. Monajjemi, M.; Mollaamin, F.; Shahriari, S.; Mohammadi, S. Synthesis of Nano C60-[Fe<sub>3</sub>O<sub>4</sub>/SiO<sub>2</sub>/GeO<sub>2</sub>] as Efficient Catalyst Disinfection. *Russ. J. Phys. Chem. B* **2024**, *18*, 1217–1225, <https://doi.org/10.1134/S1990793124700349>.
25. Monajjemi, M., Mohammadi, S., Shahriari, S.; Mollaamin, F. Experimental and Theoretical Studies of ZnO Nanotubes: an Approach to Chemical Physics Characterization of ZnONTs, Including Morphology, Piezoelectric, and Density of States. *Russ. J. Phys. Chem. B* **2024**, *18*, 308–324, <https://doi.org/10.1134/S1990793124010342>.
26. Mollaamin, F. Computational Methods in the Drug Delivery of Carbon Nanocarriers onto Several Compounds in Sarraceniaceae Medicinal Plant as Monkeypox Therapy. *Computation* **2023**, *11*, 84, <https://doi.org/10.3390/computation11040084>
27. Mollaamin, F. Investigating the Treatment of Transition Metals for Ameliorating the Ability of Boron Nitride for Gas Sensing & Removing: A Molecular Characterization by DFT Framework. *Prot. Met. Phys. Chem. Surf.* **2024**, *60*, 1050–1063, <https://doi.org/10.1134/S2070205124702502>.
28. Mollaamin, F.; Monajjemi, M. The influence of Sc, V, Cr, Co, Cu, Zn as ferromagnetic semiconductors implanted on B<sub>5</sub>N<sub>10</sub>-nanocarrier for enhancing of NO sensing: An environmental eco-friendly investigation. *Comput. Theor. Chem.* **2024**, *1237*, 114666, <https://doi.org/10.1016/j.comptc.2024.114666>.
29. Domi, B.; Bhorkar, K.; Rumbo, C.; Sygellou, L.; Yannopoulos, S.N.; Barros, R.; Quesada, R.; Tamayo-Ramos, J.A. Assessment of Physico-Chemical and Toxicological Properties of Commercial 2D Boron Nitride Nanopowder and Nanoplatelets. *Int. J. Mol. Sci.* **2021**, *22*, 567, <https://doi.org/10.3390/ijms22020567>.
30. Ghaderzadeh, S.; Kretschmer, S.; Ghorbani-Asl, M.; Hlawacek, G.; Krasheninnikov, A.V. Atomistic Simulations of Defect Production in Monolayer and Bulk Hexagonal Boron Nitride under Low- and High-Fluence Ion Irradiation. *Nanomaterials* **2021**, *11*, 1214, <https://doi.org/10.3390/nano11051214>.
31. Mballo, A.; Srivastava, A.; Sundaram, S.; Vuong, P.; Karrakchou, S.; Halfaya, Y.; Gautier, S.; Voss, P.L.; Ahaitouf, A.; Salvestrini, J.P.; Ougazzaden, A. Towards P-Type Conduction in Hexagonal Boron Nitride: Doping Study and Electrical Measurements Analysis of hBN/AlGa<sub>N</sub> Heterojunctions. *Nanomaterials* **2021**, *11*, 211, <https://doi.org/10.3390/nano11010211>.
32. Silva, W.M.; Ribeiro, H.; Taha-Tijerina, J.J. Potential Production of Theranostic Boron Nitride Nanotubes (<sup>64</sup>Cu-BNNTs) Radiolabeled by Neutron Capture. *Nanomaterials* **2021**, *11*, 2907, <https://doi.org/10.3390/nano11112907>.
33. Mollaamin, F.; Monajjemi, M. Structural, Electromagnetic and Thermodynamic Analysis of Ion Pollutants Adsorption in Water by Gallium Nitride Nanomaterial: a Green Chemistry Application. *Russ. J. Phys. Chem. B* **2024**, *18*, 533–548, <https://doi.org/10.1134/S199079312402012X>.
34. Zhao, L.-H.; Liao, Y.; Jia, L.-C.; Wang, Z.; Huang, X.-L.; Ning, W.-J.; Zhang, Z.-X.; Ren, J.-W. Ultra-Robust Thermoconductive Films Made from Aramid Nanofiber and Boron Nitride Nanosheet for Thermal Management Application. *Polymers* **2021**, *13*, 2028, <https://doi.org/10.3390/polym13132028>.
35. Lee Sanchez, W.A.; Huang, C.-Y.; Chen, J.-X.; Soong, Y.-C.; Chan, Y.-N.; Chiou, K.-C.; Lee, T.-M.; Cheng, C.-C.; Chiu, C.-W. Enhanced Thermal Conductivity of Epoxy Composites Filled with Al<sub>2</sub>O<sub>3</sub>/Boron Nitride Hybrids for Underfill Encapsulation Materials. *Polymers* **2021**, *13*, 147, <https://doi.org/10.3390/polym13010147>.
36. Shiratori, T.; Yamane, I.; Nodo, S.; Ota, R.; Yanase, T.; Nagahama, T.; Yamamoto, Y.; Shimada, T. Synthesis of Boron Nitride Nanotubes Using Plasma-Assisted CVD Catalyzed by Cu Nanoparticles and Oxygen. *Nanomaterials* **2021**, *11*, 651, <https://doi.org/10.3390/nano11030651>.

37. Güzdemir, Ö.; Kanhere, S.; Bermudez, V.; Ogale, A.A. Boron Nitride-Filled Linear Low-Density Polyethylene for Enhanced Thermal Transport: Continuous Extrusion of Micro-Textured Films. *Polymers* **2021**, *13*, 3393, <https://doi.org/10.3390/polym13193393>.
38. Mateti, S.; Sultana, I.; Chen, Y.; Kota, M.; Rahman, M.M. Boron Nitride-Based Nanomaterials: Synthesis and Application in Rechargeable Batteries. *Batteries* **2023**, *9*, 344, <https://doi.org/10.3390/batteries9070344>.
39. Mollaamin, F. Competitive Intracellular Hydrogen-Nanocarrier Among Aluminum, Carbon, or Silicon Implantation: a Novel Technology of Eco-Friendly Energy Storage using Research Density Functional Theory. *Russ. J. Phys. Chem. B* **2024**, *18*, 805–820, <https://doi.org/10.1134/S1990793124700131>.
40. Zhang, Y.; Si, H.; Liu, S.; Jiang, Z.; Zhang, J.; Gong, C. Facile synthesis of BN/Ni nanocomposites for effective regulation of microwave absorption performance. *J. Alloys Compd.* **2021**, *850*, 156680, <https://doi.org/10.1016/j.jallcom.2020.156680>.
41. Park, Y.-G.; Nam, S.-N.; Jang, M.; Min Park, C.; Her, N.; Sohn, J.; Cho, J.; Yoon, Y. Boron nitride-based nanomaterials as adsorbents in water: A review. *Sep. Purif. Technol.* **2022**, *288*, 120637, <https://doi.org/10.1016/j.seppur.2022.120637>.
42. Mollaamin, F.; Monajjemi, M. Electric and Magnetic Evaluation of Aluminum–Magnesium Nanoalloy Decorated with Germanium Through Heterocyclic Carbenes Adsorption: A Density Functional Theory Study. *Russ. J. Phys. Chem. B* **2023**, *17*, 658–672, <https://doi.org/10.1134/S1990793123030223>.
43. Anota, E.C. 2D boron nitride incorporating homonuclear boron bonds: stabilized in neutral, anionic and cationic charge. *SN Appl. Sci.* **2022**, *4*, 295, <https://doi.org/10.1007/s42452-022-05180-z>.
44. Mollaamin, F.; Monajjemi, M. Tailoring and functionalizing the graphitic-like GaN and GaP nanostructures as selective sensors for NO, NO<sub>2</sub>, and NH<sub>3</sub> adsorbing: a DFT study. *J. Mol. Model* **2023**, *29*, 170, <https://doi.org/10.1007/s00894-023-05567-8>.
45. Shtansky, D.V.; Matveev, A.T.; Permyakova, E.S.; Leybo, D.V.; Konopatsky, A.S.; Sorokin, P.B. Recent Progress in Fabrication and Application of BN Nanostructures and BN-Based Nanohybrids. *Nanomaterials* **2022**, *12*, 2810, <https://doi.org/10.3390/nano12162810>.
46. Yang, Y.; Peng, Y.; Saleem, M.F.; Chen, Z.; Sun, W. Hexagonal Boron Nitride on III–V Compounds: A Review of the Synthesis and Applications. *Materials* **2022**, *15*, 4396, <https://doi.org/10.3390/ma15134396>.
47. Mollaamin, F.; Monajjemi, M. Selectivity and Sensitivity Evaluation of Embedded BN-Nanostructure as a Gas Detector for Air Pollution Scavenging: a Theoretical Study. *Russ. J. Phys. Chem. B* **2024**, *18*, 1177–1198, <https://doi.org/10.1134/S1990793124700507>.
48. Mollaamin, F.; Monajjemi, M. Corrosion Inhibiting by Some Organic Heterocyclic Inhibitors Through Langmuir Adsorption Mechanism on the Al-X (X = Mg/Ga/Si) Alloy Surface: A Study of Quantum Three-Layer Method of CAM-DFT/ONIOM. *J. Bio- Tribo-Corros.* **2023**, *9*, 33, <https://doi.org/10.1007/s40735-023-00751-y>.
49. Dennington, R.; Keith Todd, A.; Millam John, M. GaussView, Version 6.06.16. Semichem Inc., Shawnee Mission, KS, USA, **2016**.
50. Frisch, M.J.; Trucks, G.W.; Schlegel, H.B.; Scuseria, G.E.; Robb, M.A.; Cheeseman, J.R.; Scalmani, G.; Barone, V.; Petersson, G.A.; Nakatsuji, H.; Li, X.; Caricato, M.; Marenich, A.V.; Bloino, J.; Janesko, B.G.; Gomperts, R.; Mennucci, B.; Hratchian, H.P.; Ortiz, J. V.; Izmaylov, A. F.; Sonnenberg, J.L.; Williams-Young, D.; Ding, F.; Lipparini, F.; Egidi, F.; Goings, J.; Peng, B.; Petrone, A.; Henderson, T.; Ranasinghe, D.; Zakrzewski, V.G.; Gao, J.; Rega, N.; Zheng, G.; Liang, W.; Hada, M.; Ehara, M.; Toyota, K.; Fukuda, R.; Hasegawa, J.; Ishida, M.; Nakajima, T.; Honda, Y.; Kitao, O.; Nakai, H.; Vreven, T.; Throssell, K.; Montgomery, J.A., Jr.; Peralta, J.E.; Ogliaro, F.; Bearpark, M.J.; Heyd, J.J.; Brothers, E.N.; Kudin, K.N.; Staroverov, V.N.; Keith, T.A.; Kobayashi, R.; Normand, J.; Raghavachari, K.; Rendell, A.P.; Burant, J.C.; Iyengar, S.S.; Tomasi, J.; Cossi, M.; Millam, J.M.; Klene, M.; Adamo, C.; Cammi, R.; Ochterski, J.W.; Martin, R.L.; Morokuma, K.; Farkas, O.; Foresman, J.B.; Fox, D.J. Gaussian 16, Revision C.01, Gaussian, Inc., Wallingford CT, **2016**.
51. Chang, C.M.; Chang, Y.-H. Density Functional Theory Studies on Boron Nitride and Silicon Carbide Nanoclusters Functionalized with Amino Acids for Organophosphorus Pesticide Adsorption. *Crystals* **2024**, *14*, 594, <https://doi.org/10.3390/cryst14070594>.
52. Mollaamin, F.; Shahriari, S.; Monajjemi, M. Influence of Transition Metals for Emergence of Energy Storage in Fuel Cells through Hydrogen Adsorption on the MgAl Surface. *Russ. J. Phys. Chem. B* **2024**, *18*, 398–418, <https://doi.org/10.1134/S199079312402026X>.
53. Cramer, C.J. Essentials of Computational Chemistry: Theories and Models, 2<sup>nd</sup> Edition; John Wiley & Sons, Ltd: England, **2004**.

54. Perdew, J.P.; Burke, K.; Ernzerhof, M. Generalized Gradient Approximation Made Simple. *Phys. Rev. Lett.* **1996**, *77*, 3865, <https://doi.org/10.1103/PhysRevLett.77.3865>.
55. Mollaamin, F. Alkali Metals Doped on Tin-Silicon and Germanium-Silicon Oxides for Energy Storage in Hybrid Biofuel Cells: A First-Principles Study. *Russ. J. Phys. Chem. B.* **2025**, *19*, 722–736. <https://doi.org/10.1134/S1990793125700393>.
56. Shahriari, S.; Mollaamin, F.; Monajjemi, M. Increasing the Performance of {[ $(1-x-y)$  LiCo<sub>0.3</sub>Cu<sub>0.7</sub>] (Al and Mg doped) O<sub>2</sub>}, xLi<sub>2</sub>MnO<sub>3</sub>, yLiCoO<sub>2</sub> Composites as Cathode Material in Lithium-Ion Battery: Synthesis and Characterization. *Micromachines.* **2023**, *14*, 241, <https://doi.org/10.3390/mi14020241>.
57. Ge, M.; Chu, L.; Guo, M.; Su, Y.; Zhang, J. First-Principles Study of Ir<sub>n</sub> (n = 3–5) Clusters Adsorbed on Graphene and Hexagonal Boron Nitride: Structural and Magnetic Properties. *Nanomaterials* **2022**, *12*, 2436, <https://doi.org/10.3390/nano12142436>.
58. Mollaamin, F.; Monajjemi, M. Effect of Implanted Titanium, Vanadium or Chromium on Boron Nitride Surface for Increasing Carbon Monoxide Adsorption: Designing Gas Sensor for Green Chemistry Future. *Russ. J. Phys. Chem. B* **2024**, *18*, 1199–1216, <https://doi.org/10.1134/S1990793124700519>.
59. Mollaamin, F.; Shahriari, S.; Monajjemi, M.; Khalaj, Z. Nanocluster of Aluminum Lattice via Organic Inhibitors Coating: A Study of Freundlich Adsorption. *J. Clust. Sci.* **2023**, *34*, 1547–1562, <https://doi.org/10.1007/s10876-022-02335-1>.
60. Mollaamin, F.; Monajjemi, M. Transition metal (X = Mn, Fe, Co, Ni, Cu, Zn)-doped graphene as gas sensor for CO<sub>2</sub> and NO<sub>2</sub> detection: a molecular modeling framework by DFT perspective. *J. Mol. Model* **2023**, *29*, 119, <https://doi.org/10.1007/s00894-023-05526-3>.
61. Mollaamin, F.; Monajjemi, M. Graphene-based resistant sensor decorated with Mn, Co, Cu for nitric oxide detection: Langmuir adsorption & DFT method. *Sensor Rev.* **2023**, *43*, 266–279, <https://doi.org/10.1108/SR-03-2023-0040>.
62. Mollaamin, F. Alkali Metals Doped on Tin-Silicon and Germanium-Silicon Oxides for Energy Storage in Hybrid Biofuel Cells: A First-Principles Study. *Russ. J. Phys. Chem. B* **2025**, *19*, 720–736, <https://doi.org/10.1134/S1990793125700393>.
63. Mollaamin, F.; Monajjemi, M. In Silico-DFT Investigation of Nanocluster Alloys of Al-(Mg, Ge, Sn) Coated by Nitrogen Heterocyclic Carbenes as Corrosion Inhibitors. *J. Clust. Sci.* **2023**, *34*, 2901–2918, <https://doi.org/10.1007/s10876-023-02436-5>.
64. Wang, J.; Wei, Y.; Ma, Z. Modified Dual-Site Langmuir Adsorption Equilibrium Models from A GCMC Molecular Simulation. *Appl. Sci.* **2020**, *10*, 1311, <https://doi.org/10.3390/app10041311>.
65. Wu, Z.; Ji, Y.; Zhang, K.; Jing, L.; Zhao, T. On the Use of the Multi-Site Langmuir Model for Predicting Methane Adsorption on Shale. *Energies* **2024**, *17*, 4990, <https://doi.org/10.3390/en17194990>.
66. de Souza, R.F.; de Almeida, R.R.R.; Omori, E.K.; de Souza, R.T.; Lenzi, E.K.; Evangelista, L.R.; Zola, R.S. Role of the Number of Adsorption Sites and Adsorption Dynamics of Diffusing Particles in a Confined Liquid with Langmuir Kinetics. *Physchem* **2023**, *3*, 1-12, <https://doi.org/10.3390/physchem3010001>.
67. Vigdorowitsch, M.; Pchelintsev, A.; Tsygankova, L.; Tanygina, E. Freundlich Isotherm: An Adsorption Model Complete Framework. *Appl. Sci.* **2021**, *11*, 8078, <https://doi.org/10.3390/app11178078>.
68. Mollaamin, F.; Monajjemi, M. Application of DFT and TD-DFT on Langmuir Adsorption of Nitrogen and Sulfur Heterocycle Dopants on an Aluminum Surface Decorated with Magnesium and Silicon. *Computation* **2023**, *11*, 108, <https://doi.org/10.3390/computation11060108>.
69. Mollaamin, F.; Monajjemi, M. Boron nitride doped with transition metals for carbon monoxide detection: a promising nanosensor for air cleaning. *Sensor Rev.* **2024**, *44*, 179–193, <https://doi.org/10.1108/SR-01-2024-0066>.
70. Mollaamin, F.; Monajjemi, M. Adsorption ability of Ga<sub>5</sub>N<sub>10</sub> nanomaterial for removing metal ions contamination from drinking water by DFT. *Int. J. Quantum Chem.* **2024**, *124*, e27348, <https://doi.org/10.1002/qua.27348>.
71. Lehtola, S. A review on non-relativistic, fully numerical electronic structure calculations on atoms and diatomic molecules. *Int. J. Quantum Chem.* **2019**, *119*, e25968, <https://doi.org/10.1002/qua.25968>.
72. Mollaamin, F.; Monajjemi, M. Trapping of toxic heavy metals from water by GN–nanocage: Application of nanomaterials for contaminant removal technique. *J. Mol. Struct.* **2024**, *1300*, 137214, <https://doi.org/10.1016/j.molstruc.2023.137214>.
73. Mollaamin, F.; Monajjemi, M. In Situ Ti-Embedded SiC as Chemiresistive Nanosensor for Safety Monitoring of CO, CO<sub>2</sub>, NO, NO<sub>2</sub>: Molecular Modelling by Conceptual Density Functional Theory. *Russ. J. Phys. Chem. B* **2024**, *18*, 49–66, <https://doi.org/10.1134/S1990793124010159>.

74. Huang, T.; Miao, C.; Wan, S.; Tian, X.; Li, R. A Fast and Efficient Measurement System for Nuclear Spin Relaxation Times in Atomic Vapors. *Sensors* **2019**, *19*, 4863, <https://doi.org/10.3390/s19224863>.
75. Monajjemi, M.; Mollaamin, F.; Shahriari, S. Khalaj, Z.; Sakhaeinia, H.; Alihosseini, A. Interaction of Nano-Boron Nitride Sheets with Electrodes in Lithium Ion Battery for Increasing Voltage and Amperage. *Russ. J. Phys. Chem. B.* **2024**, *18*, 1090–1112, <https://doi.org/10.1134/S1990793124700465>.

### **Publisher's Note & Disclaimer**

The statements, opinions, and data presented in this publication are solely those of the individual author(s) and contributor(s) and do not necessarily reflect the views of the publisher and/or the editor(s). The publisher and/or the editor(s) disclaim any responsibility for the accuracy, completeness, or reliability of the content. Neither the publisher nor the editor(s) assume any legal liability for any errors, omissions, or consequences arising from the use of the information presented in this publication. Furthermore, the publisher and/or the editor(s) disclaim any liability for any injury, damage, or loss to persons or property that may result from the use of any ideas, methods, instructions, or products mentioned in the content. Readers are encouraged to independently verify any information before relying on it, and the publisher assumes no responsibility for any consequences arising from the use of materials contained in this publication.